Embedding a Magnetoelastic Material Model in a Coupled Magnetomechanical Finite-Element Solver

Dries Vanoost[1,2], Simon Steentjes[3], Herbert De Gersem[2,4], Joan Peuteman[1,5], Georges Gielen[6], Davy Pissoort[1,6], and Kay Hameyer[3]

[1]ReMI Research Group, Katholieke Universiteit Leuven Technology Campus Ostend, Oostende B-8400, Belgium
[2]Wave Propagation and Signal Processing Research Group, Katholieke Universiteit Leuven Kulak, Kortrijk B-8500, Belgium
[3]Institute of Electrical Machines, RWTH Aachen University, Aachen D-52062, Germany
[4]Institut für Theorie Elektromagnetischer Felder, Technische Universität Darmstadt, Darmstadt D-64289, Germany
[5]Department of Electrical Engineering, Electrical Energy and Computer Architecture, Katholieke Universiteit Leuven, Heverlee B-3000, Belgium
[6]Department of Electrical Engineering, Microelectronics and Sensors, Katholieke Universiteit Leuven, Heverlee B-3000, Belgium

This paper proposes a magnetomechanical 2-D finite-element solver embedding an energy-based material model. The energy-based material model determines the value of the permeability tensor in each material point of the computational grid based on the material data, the magnetic field strength, and the mechanical stress. The simulation results are compared with the measurement data for a nickel I-beam benchmark.

Index Terms— **Finite-element (FE) analysis, magnetomechanical effects, nonlinear magnetics, partial differential equations.**

I. Introduction

THE Villari effect, also called the inverse magnetostrictive effect, describes the influence of a mechanical stress on the magnetic permeability [7], [8]. The stress can be internal or external, e.g., the stress can be induced by the manufacturing process [6], by heating or cooling, or by the assembly process. The Villari effect has a substantial influence on the magnetic behavior of electrical energy transducers. For many devices, magnetostriction should be considered during the design process [11]. The Villari effect can also be used as a working principle, e.g., in magnetoelectric tunable inductors [14].

When a significant Villari effect occurs, a reliable magnetomechanical field simulation procedure capable of embedding an energy-based material model is needed. The spatial inhomogeneity of the mechanical stress implies a spatial inhomogeneity of the magnetic permeability. Hence, a volumetric discretization as provided by the finite-element (FE) method is mandatory. Moreover, not only the spatial resolutions of the mechanical and magnetic field quantities but also the spatial resolutions of the material parameters become an issue. In this paper, a 2-D coupled magnetomechanical FE simulation scheme is set up, a generic interface to an energy-based material model is discussed, and an appropriate way to guide the spatial resolutions is pointed out. The solver coupling is implemented using commonly available tools. Simulation results obtained with the coupled solver in combination with a simple, energy-based material model are compared with the new measurement data.

Manuscript received March 20, 2015; revised May 22, 2015; accepted May 28, 2015. Date of publication June 1, 2015; date of current version October 22, 2015. Corresponding author: D. Vanoost (e-mail: dries.vanoost@kuleuven-kulak.be).

Color versions of one or more of the figures in this paper are available online at http://ieeexplore.ieee.org.

Digital Object Identifier 10.1109/TMAG.2015.2439954

II. Coupled Magnetomechanic Field Simulation

The governing partial differential equations are

$$-\nabla \cdot (\mathbf{Y}(\sigma, \mathbf{H})\nabla \mathbf{u}) = \mathbf{f} \tag{1}$$

$$\nabla \times (\nu(\mathbf{H}, \sigma)\nabla \times \mathbf{A}) = \mathbf{J} \tag{2}$$

where the Young modulus $\mathbf{Y}$ relates the strain $\varepsilon = \mathbf{Y}\sigma$ to the stress σ, the reluctivity ν relates the magnetic field strength $\mathbf{H} = \nu\mathbf{B}$ to the magnetic flux density $\mathbf{B}$, $\mathbf{u}$ is the displacement, $\mathbf{f}$ is the force density, $\mathbf{A}$ is the magnetic vector potential, and $\mathbf{J}$ is the current density [13]. Because of the Villari effect, both the elastic and magnetic material properties of $\mathbf{Y}(\sigma, \mathbf{H})$ and $\nu(\mathbf{H}, \sigma)$ depend on the mechanical and magnetic fields. When, however, the σ dominates over $\mathbf{H}$, the impact on $\mathbf{Y}$ is less pronounced and can be neglected. In this case, the dependence of ν on both the magnetic field strength $\mathbf{H}$ and the mechanical stress σ is relevant and needs to be considered. To that purpose, an iterative process is set up (Fig. 2). The computational cost can be reduced by leaving the mechanical simulation out of the iteration process. Indeed, these simulations would always lead to the same results because $\mathbf{Y}$ stays more or less constant.

In further iteration steps, the stress is kept constant, whereas the reluctivities are successively updated according to the intermediately obtained magnetic field strengths. The application allows us to use 2-D models. To obtain an accurate and efficient magnetomechanical solver, three independent computational meshes are used, i.e., two fine meshes for the mechanical and magnetic field solvers which are adapted to strong local variations of the respective fields, and one coarse mesh, embedded in both other meshes, for evaluating the material model. This coarsening is important to achieve a sufficiently fast overall simulation scheme. The coarse material mesh of the magnetostrictive model region consists of quadrilaterals. The displacement and the magnetic vector potential are discretized at the cross-sectional plane by the

second-order and the first-order nodal FEs, respectively. The material properties are piecewise constant.

III. Magnetoelastic Material Model

A suitable material model is selected depending on the available material data and the required accuracy and efficiency. Phenomenological macroscopic and micromagnetic material models are distinguished. In phenomenological macroscopic material models, the stress is introduced as a parameter in a classical macroscopic hysteresis model such as the Jiles–Atherton–Sablik model [18] or the Preisach model [2]. These material models are comparably simple and enable fast computations, but are inappropriate when intended for studying and optimizing devices with severe magnetostriction. This is because they mostly do not account for multiaxial stress situations. Material models based on micromagnetic simulations require more fundamental material parameters defined at the crystal and/or grain scale, but are comparably heavy. The effect of mechanical stresses on the magnetic domain behavior is found by minimizing energy functions representing the potential energy of single crystals or grains [3], [10], [15], [19]. The macroscopic behavior is found by upscaling (homogenizing) the microscopic material parameters to the macroscopic level. Daniel *et al.* the authors of [9] proposed a multiscale approach for magnetoelasticity which enables the use of the micromagnetic simulations in macroscale models of, e.g., electric machines and transformers. This paper uses the Armstrong model [3] as an example for embedding energy-based material models in a magnetomechanical FE solver. Further improvements to energy-based material models have been proposed in [4] and [5] and can be introduced in the proposed magnetomechanical solver similarly.

The magnetic field strength $\mathbf{H}_i$ in the coarse-mesh element i causes a magnetization $\mathbf{M}_i$ for which the total energy W_{tot} is minimal. The total energy W_{tot} is the sum of the Zeeman energy W_H, the magnetocrystalline anisotropy energy W_{an}, and the stress-induced anisotropy energy W_σ [3]. W_{tot} is minimized for every coarse-mesh element i independently. A number of possible magnetizations $\mathbf{M}_i = (\alpha_1, \alpha_2, \alpha_3)M_s$ with saturation magnetization M_s and its direction cosines $\alpha = (\alpha_1, \alpha_2, \alpha_3)$ with respect to the crystal structure, are considered. The discretization of the parameter space for α corresponds to the discretization of a spherical surface. The Zeeman energy $W_H = -\mu_0 \mathbf{M}_i \cdot \mathbf{H}_i$ is minimized when $\mathbf{H}_i$ is aligned with $\mathbf{M}_i$. The magnetocrystalline anisotropy, $W_{\text{an}} = K_1(\alpha_1^2\alpha_2^2 + \alpha_2^2\alpha_3^2 + \alpha_3^2\alpha_1^2) + K_2\alpha_1^2\alpha_2^2\alpha_3^2$, with the crystal anisotropic constants K_1 and K_2 models the energy increase occurring when the magnetization is not aligned with any of the easy axes. The stress induced anisotropy energy $W_\sigma = -(3/2)\lambda_{100}[\sigma_{11}(\alpha_1^2 - (1/3)) + \sigma_{22}(\alpha_2^2 - (1/3)) + \sigma_{33}(\alpha_3^2 - (1/3))] - 3\lambda_{111}[\sigma_{12}\alpha_1\alpha_2 + \sigma_{23}\alpha_2\alpha_3 + \sigma_{31}\alpha_3\alpha_1]$, with the saturation magnetostrictions λ_{100} and λ_{111}, models the effect of the applied stress. Crystal imperfections are introduced in the model by a Boltzmann distribution yielding a direction probability $P_\alpha = e^{W_{\text{tot}}/\xi} / \int_\alpha e^{W_{\text{tot}}/\xi}$, where $0 \leq \xi < +\infty$ indicates the level of perfection. The magnetization direction of coarse-mesh element i is then found by $\alpha_i = \int_{\alpha'} P_\alpha(\alpha')\alpha \, \mathrm{d}\alpha'$. The corresponding magnetization is $\mathbf{M}_i = M_s\alpha_i$. The material model is implemented in MATLAB. The probability distribution according to the possible magnetization directions is shown for polycrystalline nickel [8] with saturation magnetization $M_s = 484$ kA/m, crystal anisotropic constants $K_1 = -5$ kJ/m^3 and $K_2 = -2$ kJ/m^3, saturation magnetostrictions $\lambda_{100} = -46$ μm/m and $\lambda_{111} = -24$ μm/m, and parameter $\xi = 300$ and Young's modulus $Y = 205$ GPa, evaluated for an exemplary operating point in Fig. 1.

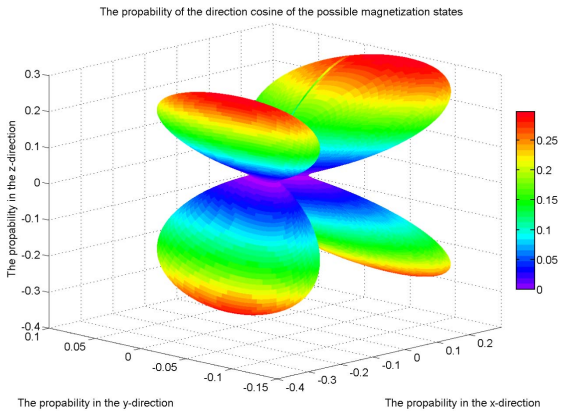

Fig. 1. Probability distribution according to the possible magnetization directions for polycrystalline nickel [8] with saturation magnetization $M_s = 484$ kA/m, crystal anisotropic constants $K_1 = -5$ kJ/m^3 and $K_2 = -2$ kJ/m^3, saturation magnetostrictions $\lambda_{100} = -46$ μm/m and $\lambda_{111} = -24$ μm/m, and parameter $\xi = 300$ and Young's modulus $Y = 205$ GPa, evaluated for the magnetic field strength $\mathbf{H} = (1, -1000, 1)$ A/m and the stress $\sigma = (0.1, 70, 0.1, 0, 0, 0)$ MPa (Voigt notation). The azimuth and inclination defining the cosine directions are discretized in steps of 1°.

IV. Embedding Material Model in FE Field Solver

After a field solution by the FE solver, values $\sigma^{(k)}(x_i, y_i)$ and $\mathbf{H}^{(k)}(x_i, y_i)$ for iteration step k are obtained by averaging the field solutions at the center points (x_i, y_i) of the coarse-mesh elements Ω_i, $i = 1, \ldots, N$ with N the number of coarse-mesh elements. Then, N micromagnetic simulations are carried out, one per coarse-mesh element. The magnetic field solutions $\mathbf{H}_i^{(k)}$ allow us to determine the material relation $\mathbf{B} = \mu_0(\mathbf{H} + \mathbf{M}_i^{(k)})$ to be used for the next iteration $k+1$. This procedure is equivalent to a polarization approach which is known to converge slowly, especially for highly permeable materials [12]. A faster convergence is expected when using a successive substitution approach. To that purpose, three direction-dependent permeabilities $\mu_{i,d}^{(k)}$, $d \in \{1, 2, 3\}$ are calculated by

$$\mu_{i,d}^k = \begin{cases} \mu_0 \left(1 + \dfrac{M_S \alpha_{i,d}^{(k)}}{H_{i,d}^{(k)}}\right) & \text{if } H_{i,d}^k > H_{\text{tol}} \\ \mu_0 & \text{if } H_{i,d}^k \leq H_{\text{tol}} \end{cases}, \tag{3}$$

with tolerance $H_{\text{tol}} = 1$ A/m. The material relation considered by the magnetic field solver for coarse-mesh element i in iteration step $k+1$ is then $\mathbf{H} = \text{diag}((1/\mu_{i,1}^{(k)}), (1/\mu_{i,2}^{(k)}), (1/\mu_{i,3}^{(k)}))\mathbf{B}$. The convergence of the iteration is measured according to the values for $\mu_{i,d}$. When $|\mu_{i,d}^{(k)} - \mu_{i,d}^{(k-1)}| < 0.01\mu_{i,d}^{(k)}$, $\forall d$ and $\forall i$, the iteration is stopped. Numerical experiments indicate that this iteration converges even without relaxation. In general, the Newton method is known to provide a better convergence than the successive substitution approach [16]. However, the calculation of the required differential material properties is prohibitively difficult for this application.

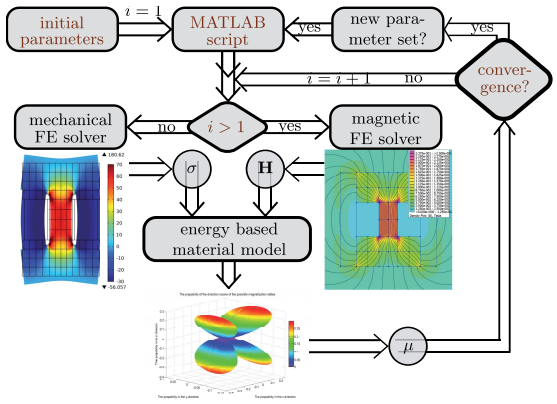

Fig. 2. Flowchart of the magnetomechanical FE solver.

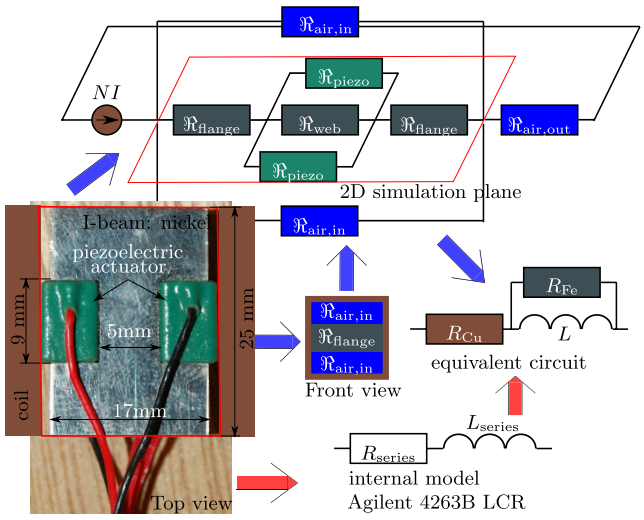

Fig. 3. Test setup with its magnetic and electric equivalent circuit.

V. Test Case

A little nickel I-beam (Fig. 3) is used as a benchmark. Nickel features negative magnetostriction [8], has a relatively large Young modulus [1], exhibits a substantial Villari effect [8], and is relatively easy to shape. The choice for negative magnetostriction is motivated by the fact that the permeability decrease due to tension is typically larger than the permeability increase due to a comparable compression. The material data have already been listed in Section III. The required tension is generated by two piezoelectric actuators of type PSt 150/5 × 5/7 [17] fixed between the flanges of the I-beam and fed by a dc voltage source (type Hp 6030A System Power Supply 0–200 V/0–17 A/100 W). The I-beam is mounted inside a measurement coil with 800 turns, an inner section of 19.7 mm × 19.5 mm, and a length of 23 mm. The applied stresses cause a permeability change of the nickel, which is measured as a change of the coil inductance (Fig. 5). A positive voltage causes a stretching of the I-beam web, an according decrease of the permeability leading to a decrease of the coil inductance. The coil impedance is measured by an Agilent 4263B *LCR* meter at a frequency $f = 100$ Hz. The measured impedance values $Z = R_{\text{series}} + \jmath\omega L_{\text{series}}$ with $\omega = 2\pi f$ the angular frequency are transferred into coil inductance L according to the equivalent circuit shown

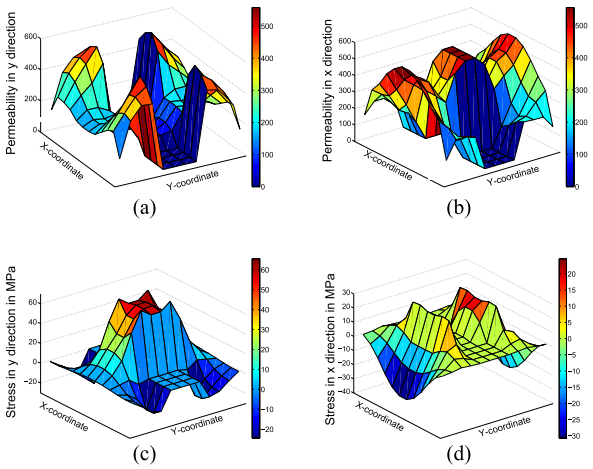

Fig. 4. Simulated (a) relative permeability in the y-direction, (b) relative permeability in the x-direction, (c) stress in the y-direction, and (d) stress in the x-direction, using a dc-voltage of 150V for the piezoelectric actuators.

in Fig. 3, by the formula

$$L = L_{\text{series}} + \frac{(R_{\text{series}} - R_{Cu})^2}{\omega^2 L_{\text{series}}} \tag{4}$$

with R_{Cu} the coil resistance, measured separately. The measured change of inductance as a function of the dc-voltage applied to the piezoelectric actuators is shown in Fig. 5. The measurement procedure started at a dc-voltage of 10 V and follows two cycles with steps of 10 V, up to 150 V, down to −30 V and back to 0 V. After every change of the dc-voltage, the coil inductance L is determined.

The measurement data serve as a reference for the numerical model. The magnetomechanical FE solver calculates the stress distribution for a given dc-voltage applied to the piezoelectric actuators. Fig. 4 shows the spatial distributions of stresses and permeabilities. The magnetic field is mainly oriented along the y-direction. The tension in the I-beam web leads to a decrease of the permeability along the vertical y-direction and an increase of the permeability along the x-direction. The complicated stress distribution in the flanges and at the corner points causes nontrivial spatial distributions of the permeabilities. Without mechanical load, nickel has an isotropic permeability. The applied stresses introduce a remarkably high level of anisotropy in the sample.

The magnetomechanical field solver is applied for a 2-D cross-sectional model of the I-beam and the piezoelectric actuators (Fig. 3). The resulting permeability distribution allows us to calculate the reluctance $\Re_{\text{sample}} = 2\Re_{\text{flange}} + (\Re_{\text{web}} \mathbin{/\!/} 2\Re_{\text{piezo}})$, where $/\!/$ indicates a parallel connection. $\Re_{\text{flange}}$, $\Re_{\text{web}}$, and $\Re_{\text{piezo}}$ are the reluctances of the vertical magnetic flux paths through the I-beam's flanges and web and through the piezoelectric parts, respectively. The reluctances $\Re_{\text{air,in}}$ of the air fractions around the I-beam (see front view of Fig. 3) are calculated analytically. The reluctance $\Re_{\text{air,out}}$ of the closing path outside the coil is found by 3-D FE simulation. Then, the coil inductance follows from:

$$L_{\text{simu}} = \frac{N^2}{\Re_{\text{sample}} \mathbin{/\!/} \Re_{\text{air,in}} + \Re_{\text{air,out}}}. \tag{5}$$

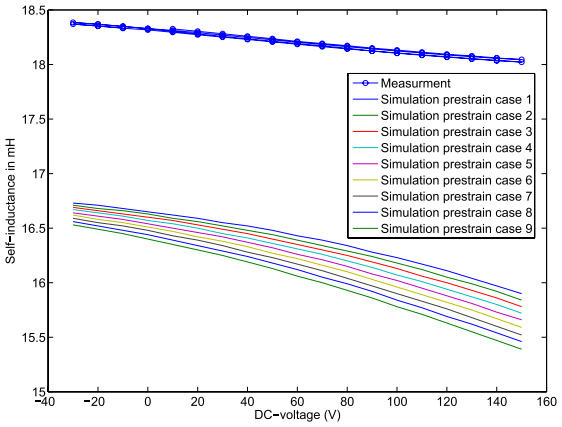

Fig. 5. Measurement data versus simulation data.

Several assumptions are made in the mechanical, magnetic, and material models.

1) In the mechanical model, the piezoelectric actuators are assumed to be identical. Moreover, slightly different flange geometries may cause an asymmetry in the applied stresses. These effects are minimized by applying wire electrical discharge machining which is able to achieve a manufacturing precision of 10 μm. The piezoelectric actuators are inserted using press fitting. As a consequence, the stroke of the actuator is defined by the I-beam material. Given an accurate machining and a homogeneous nickel piece, a sufficiently large and symmetric stress is obtained. The internal stress is reduced by a curing treatment, after machining the I-beam. The pretensions, due to the press fitting, cannot be removed, to avoid damaging the piezoelectric actuators, but they can be reduced by applying a negative dc-voltage, as shown in Fig. 5. Indeed, the inductance L increases when reducing the prestress by shrinking the piezoelectric actuators using a negative dc-voltage.
2) The simple energy-based material model is assumed to be valid for nickel, although the material model does not account for texture or internal stresses. After machining, the nickel I-beam is annealed in order to reduce crystal imperfections. Nevertheless, residual material defects cannot be excluded.
3) The main assumption in the magnetic model is the reduction of the inherently 3-D geometry to a 2-D model combined with a magnetic equivalent circuit. Because of neglecting some of the fringing field effects, the simulated inductance is underestimated.

Fig. 5 shows a systematic offset between the simulation results and the measurement data. The unknown prestrain situation is excluded as a single cause by repeating the simulations for different artificial prestrain settings (Fig. 5). Moreover, some material defects may not be healed by the annealing process, since the dependence of the Young's modulus on the magnetic field is neglected, the 3-D geometry is treated by a 2-D FE model and, most probably, the values for M_s, K_1, K_2, λ_{100} or λ_{111} are inappropriate for the used polycrystalline nickel material due to the exclusion of the orientation distribution function. The measurement and simulation data, however, share the same order of magnitude and show the same qualitative behavior.

VI. Conclusion

An energy-based material model has been embedded in a magnetomechanical coupled FE solver. The Villari effect in a nickel I-beam has been simulated and measured. A qualitative agreement is found. The computational efficiency of the coupled field simulation approach is enhanced using three independent meshes with a rather coarse mesh of material evaluation points and by organizing a successive substitution approach.

Acknowledgment

This work was supported by the Agency for Innovation by Science and Technology in Flanders.

References

[1] Special Metals, "Nickel200/201," Special Metals Corporation, Huntington, WV, USA, Tech. Rep., 2008. [online] Available: www.specialmetals.com
[2] C. Appino, G. Durin, V. Basso, C. Beatrice, M. Pasquale, and G. Bertotti, "Effect of stress anisotropy on hysteresis and Barkhausen noise in amorphous materials," *J. Appl. Phys.*, vol. 85, no. 8, pp. 4412–4414, 1999.
[3] W. D. Armstrong, "The magnetization and magnetostriction of $Tb_{0.3}Dy_{0.7}Fe_{1.9}$ fiber actuated epoxy matrix composites," *Mater. Sci. Eng. B*, vol. 47, no. 1, pp. 47–53, 1997.
[4] W. D. Armstrong, "An incremental theory of magneto-elastic hysteresis in pseudo-cubic ferro-magnetostrictive alloys," *J. Magn. Magn. Mater.*, vol. 263, nos. 1–2, pp. 208–218, 2003.
[5] J. Atulasimha, G. Akhras, and A. B. Flatau, "Comprehensive three dimensional hysteretic magnetomechanical model and its validation with experimental ⟨110⟩ single-crystal iron-gallium behavior," *J. Appl. Phys.*, vol. 103, no. 7, p. 07B336, 2008.
[6] M. Bali, H. De Gersem, and A. Muetze, "Finite-element modeling of magnetic material degradation due to punching," *IEEE Trans. Magn.*, vol. 50, no. 2, Feb. 2014, Art. ID 7018404.
[7] R. M. Bozorth, *Ferromagnetism* (The Bell Telephone Laboratories Series), 6th ed. New York, NY, USA: Van Nostrand, 1968.
[8] B. D. Cullity and C. D. Graham, *Introduction to Magnetic Materials*, 2nd ed. New York, NY, USA: Wiley, 2008.
[9] L. Daniel, O. Hubert, N. Buiron, and R. Billardon, "Reversible magneto-elastic behavior: A multiscale approach," *J. Mechan. Phys. Solids*, vol. 56, no. 3, pp. 1018–1042, 2008.
[10] A. DeSimone, R. V. Kohn, S. Müller, and F. Otto, "Magnetic microstructures: A paradigm of multiscale problems," in *Proc. Int. Congr. Ind. Appl. Math. (ICIAM)*, 2000, pp. 175–190.
[11] R. Girgis, M. Bernesjo, S. Thomas, J. Anger, D. Chu, and H. Moore, "Development of ultra—Low noise transformer technology," in *Proc. IEEE Power Energy Soc. General Meeting*, Jul. 2011, pp. 1–8.
[12] F. I. Hantila, G. Preda, and M. Vasiliu, "Polarization method for static fields," *IEEE Trans. Magn.*, vol. 36, no. 4, pp. 672–675, Jul. 2000.
[13] M. Kaltenbacher, *Numerical Simulation of Mechatronic Sensors and Actuators*. Berlin, Germany: Springer-Verlag, 2004.
[14] J. Lou, D. Reed, M. Liu, and N. X. Sun, "Electrostatically tunable magnetoelectric inductors with large inductance tunability," *Appl. Phys. Lett.*, vol. 94, no. 11, p. 112508, 2009.
[15] L. Néel, "Les lois de l'aimantation et de la subdivision en domaines élémentaires d'un monocristal de fer," (in French) *J. Phys. Radium*, vol. 5, no. 12, pp. 265–276, 1944.
[16] J. Nocedal and S. Wright, *Numerical Optimization* (Springer Series in Operations Research), 1st ed. New York, NY, USA: Springer-Verlag, 1999.
[17] L. Pickelmann, *Low Voltage Co-Fired Multilayer Stack, Rings and Chips for Actuation*. Munich, Germany: Piezomechanik, 2004. [Online]. Available: http://www.piezomechanik.com
[18] M. J. Sablik and D. C. Jiles, "Coupled magnetoelastic theory of magnetic and magnetostrictive hysteresis," *IEEE Trans. Magn.*, vol. 29, no. 4, pp. 2113–2123, Jul. 1993.
[19] J. B. Thoelke and D. C. Jiles, "Model calculation for determining local energy minima in the orientation of magnetic domains in terbium-dysprosium-iron single crystals," *J. Magn. Magn. Mater.*, vols. 104–107, pp. 1453–1454, Oct. 1992.